Metastable states in the planar two-dimensional *XY* model and dissipation in superfluid flow

G. G. Batrouni
Department of Physics, NTNU, N-7491 Trondheim, Norway and Institut Non-Linéaire de Nice, Université de Nice-Sophia Antipolis, 1361 Route des Lucioles, 06560 Valbonne, France

(Received 18 June 2004; published 17 November 2004)

We use the Metropolis algorithm to study the stability of superfluid flow in a model system, namely the two-dimensional planar *XY* model. Flow properties are examined by studying the behavior of the system in metastable "twisted" states. We demonstrate the stability of superfluidity in this model and we discuss the Meissner effect and velocity quantization. We also study the critical velocity and dissipation by vortex creation and rotational flow and their dependence on the geometry of the system. An expression for the average superfluid velocity as a function of time, $\overline{v_s}(t)$, is obtained and compared with experimental results.

DOI: 10.1103/PhysRevB.70.184517 PACS number(s): 67.40.Hf, 03.75.Kk, 05.50.+q, 67.57.Hi

I. INTRODUCTION

Interest in superfluidity has never waned. Quite the contrary, since the experimental realization of trapped atomic Bose-Einstein condensates[1,2] (BEC) activity in this field has intensified dramatically and the recent apparent discovery of a supersolid phase in solid helium[3] will most likely increase the level of interest. In addition, there is intense interest in the low temperature properties of bosons where many questions remain concerning the phase diagrams of model systems and the phase transitions from the superfluid phase to various exotic phases.

An important question concerning superfluids is that of dissipation and the critical velocity. Perhaps one of the first things one thinks of at the mention of superfluidity is "flow without friction." Very early on, Landau[4] realized that the superfluid can be treated as a dilute gas of noninteracting quasiparticle excitations (phonons) and obtained the famous and often cited Landau stability criterion for superfluids:[5]

$$v_c^L = \min_k[\omega(k)/k]. \tag{1}$$

The dispersion relation, $\omega(k)$, is the energy of a quasiparticle excitation of momentum $\hbar k$ in the fluid, and v_c^L is the *Landau critical velocity* above which dissipation sets in. Clearly, if the dispersion relation $\omega(k)$ is linear, at least for small k, the Landau critical velocity is finite. On the other hand, $v_c^L=0$ for quadratic dependence of $\omega(k)$ on k. When $v_c^L \neq 0$, dissipationless flow at finite velocity is possible and the superfluid is said to be "stable."

To measure the critical velocity of a superfluid such as liquid ^{4}helium at a temperature $T<T_\lambda=2.18$ K, one might, for example, pull an object through the superfluid: The velocity at which a drag force starts to act on this object can be thought of as a critical velocity. Such experiments have been done[6] and find a critical velocity which depends on the superfluid density, ρ_s, but not on the geometry of the system. Furthermore, this critical velocity was found to be of the order of a few tens of meters/second which is in good agreement with the Landau prediction, Eq. (1), when applied to helium.

Another way to measure the critical velocity is to set the superfluid in motion in a tube (or through an orifice) and measure the superflow velocity at which dissipation sets in. This is perhaps more appealing physically than the first experiment because it involves a flowing superfluid and because one may make connections with persistent currents observed in superconducting systems. Such flow experiments have also been performed[7] and find that the critical velocity is of the order cm/s or less and *does* depend on the size of the orifice! In addition, it was found that the higher critical velocities are obtained with the smaller orifices which is perhaps counterintuitive. These results are surprising when compared with the Landau prediction. It is thus clear experimentally that these "critical" velocities are not equivalent.

The widespread application of the Landau criterion as a test of stability, Eq. (1), has been criticized[8,9] because it applies to the case of an object moving in the fluid and not to the case of the fluid itself flowing through orifices or in a torus. Perhaps a reason for the ubiquity of the Landau criterion is that in many cases one can calculate, if only approximately, the dispersion relation $\omega(k)$. It is much more difficult to calculate, even numerically, the critical velocity observed in flow experiments.

In this paper, we shall adopt the viewpoint of reference[9] and after a brief review, we shall present our simulation. As usual, we have in mind here the two-fluid model of superfluids. In the superfluid phase, the total density ρ is the sum of two densities:

$$\rho = \rho_n + \rho_s, \tag{2}$$

where ρ_n (ρ_s) is the normal (super) fluid density. The superfluid component does not carry entropy and flows without dissipation. The total particle current is then

$$\mathbf{j} = \rho_s \mathbf{v}_s + \rho_n \mathbf{v}_n, \tag{3}$$

where $\mathbf{v}_s$ ($\mathbf{v}_n$) is the velocity of the superfluid (normal) component. To obtain the expression for $\mathbf{v}_s$, we write the superfluid wave function as

$$\psi(\mathbf{r}) = \mathrm{e}^{i\theta(\mathbf{r})}\psi_0(\mathbf{r}), \tag{4}$$

where $\psi_0(\mathbf{r})$ is real. Then,

$$\mathbf{v}_s = \langle\psi|\frac{\hat{p}}{m}|\psi\rangle = \frac{\hbar}{m}\langle\nabla\theta\rangle, \tag{5}$$

where $\hat{p}$ is the momentum operator. The superfluid velocity is proportional to the average gradient of the phase of the wave function: Clearly, if the phase does not change coherently throughout the volume of the system, $\mathbf{v}_s = 0$.

Following Ref. 9, we consider two situations which demonstrate fundamental defining properties of the superfluid.

(1) A torus containing liquid ^{4}He at $T > T_\lambda$ is spun around its axis at very low angular velocity.[10] Eventually the liquid will come to equilibrium with the moving walls. Reducing T below T_λ, the liquid goes into its superfluid phase and the superfluid component is observed to come to rest and, to conserve angular momentum, the torus and normal fluid gain angular momentum. The experiment[11] demonstrates the analog of the *Meissner effect* in superconductors.

(2) Starting with the same setup as above, the torus is spun at high angular velocity.[10] The temperature is then reduced below T_λ and the torus brought to rest. Eventually the normal component will itself reach equilibrium with the walls and come to rest. It can then be verified that the angular momentum of the stationary torus is nonzero: The superfluid component is still flowing and may continue to do so for a very long time. This is the phenomenon of persistent dissipationless flow similar to persistent currents in superconductors. Such experiments have been done by several groups, see for example Refs. 12 and 13.

These two fundamental properties may be understood with the aid of the velocity quantization condition first proposed by Onsager[14]

$$\oint \mathbf{v}_s \,.\, \mathrm{d}\mathbf{l} = n\kappa_0, \tag{6}$$

where $\kappa_0 = h/m$ is the flux quantum, h is Planck's constant and m the particle mass. Clearly, the closed integration path must enclose a "hole" in the system, either a vortex or a physical hole, otherwise the path can be shrunk continuously to a point and only $n=0$ survives. Another important property of superflow, which will come into play below, is that it is irrotational:

$$\nabla \times \mathbf{v}_s = 0. \tag{7}$$

Equation (6) demands that persistent flow take place at a well defined value $n\kappa_0$. This is not an equilibrium situation since the superfluid can reduce its free energy by coming to rest. The persistence of the flow, at least for v_s below a critical value, means that the fluid is in a *metastable* state which will eventually decay into the equilibrium stable state at rest.[9,15] As we shall see, the lifetime of this metastable state depends on the velocity itself and on T. Figure 1 shows qualitatively the form of the free energy as a function of velocity.[9,15] This also makes clear that transitions between local minima should be possible and lead to the loss of superfluid momentum, in other words the beginning of dissipation due to excessive velocity. Such phase slips were indeed observed experimentally.[16] We now make precise what was meant by "low" and "high" velocities in the discussion of the two experiments above. The Meissner effect takes place when the initial velocity corresponds to less than half a quantum and the superfluid, seeking the nearest velocity satisfying Eq. (6), comes to rest, i.e., excludes all flux. When the initial velocity is high, i.e., larger than half a quantum, the superfluid will seek the nearest velocity satisfying Eq. (6) and settle into the corresponding metastable state.

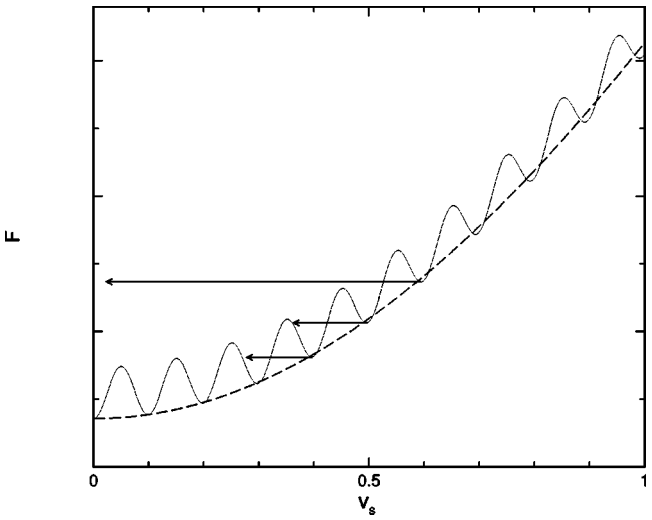

FIG. 1. Qualitative form of the free energy (arbitrary units) vs velocity in the presence of superfluidity for a 64×64 system. When the velocity satisfies Eq. (6), the free energy has a local minimum (for the values of v_s shown) which explains the metastability of persistent superfluid flow and the Meissner effect. As v_s increases, the corresponding local minima get shallower and eventually disappear rendering the flow unstable. The arrows illustrate possible transitions from local minima.

It was suggested[14,17] that vortex formation is behind these transitions and although this mechanism is generally accepted, the details are still not well understood and no numerical simulations have been done.

In the following sections we shall address these questions numerically for a model system. The paper is organized as follows. In Sec. II we briefly review the two dimensional *XY* model. In Sec. III we present our results for the nonequilibrium simulations including velocity quantization, superfluid density, transitions and flux dissipation, scaling of lifetimes with the geometry of the system and comparisons with experiments. Conclusions are in Sec. IV.

II. MODEL

Addressing these questions with quantum Monte Carlo simulations of ^{4}He or of model systems such as the bosonic Hubbard model, poses very difficult algorithmic problems. As discussed above, putting the superfluid in motion requires a gradient in the phase of the wave function. This introduces a complex phase in the Boltzmann weight rendering the simulation extremely difficult.

Instead, we shall use classical Monte Carlo to simulate the two dimensional planar *XY* model which has been studied extensively in connection with two-dimensional superfluidity. This model exhibits the well known Kosterlitz–Thouless

(KT) transition at T_{KT}. For $T>T_{\mathrm{KT}}$, there is a condensation of dissociated vortices, the phase is disordered and the correlation function decays exponentially. For $T<T_{\mathrm{KT}}$ it has a spin-wave phase characterized by tight binding of vortex–antivortex pairs and power law correlation function. There is no symmetry breaking in this phase and, therefore, no magnetization. In the language of superfluids, the absence of magnetization is equivalent to the absence of BEC. In addition, the low energy excitations, the spin waves, have a quadratic dispersion relation: $\omega(\mathbf{k})\sim\mathbf{k}^2$. On the face of it, this might be taken to imply an unstable superfluid according to the Landau criterion. However, it must be recalled the these spin waves are thermodynamic in nature, not dynamic: This model has no intrinsic dynamics, unlike the three component *XY* model which has been shown to posses dynamic spin wave excitations with linear dispersion.[18]

One may justify using this model to study the dissipation properties of two-dimensional superfluids by recalling that experiments on ^{4}He films[19] show that the transition to the superfluid phase is indeed in the KT universality class and that these films have finite critical velocity.[13,20] In addition, most explanations of dissipation in superfluid flow[21–24] are based on vortex formation which is certainly a defining property of the two-dimensional *XY* model. It is, therefore, reasonable to use this model to address the questions of superfluid stability and dissipation. The quadratic dispersion of the low-lying excitations and the absence of BEC make these questions even more interesting.

Consider, therefore, a two-dimensional square lattice with $N=L_x\times L_y$ sites. The partition function of the *XY* model is then given by

$$Z=\int_{-\pi}^{+\pi}\prod_{i=1}^{N}d\theta_i\exp\left(\beta\sum_{\langle ij\rangle}\cos(\theta_i-\theta_j)\right), \tag{8}$$

where $\langle ij\rangle$ denotes nearest neighbor sites and $\beta=1/kT$ with k the Boltzmann constant. Since the superfluid component does not carry any entropy, the increase in free energy when the superfluid is in motion is due only to its kinetic energy. Then, with ρ_s the superfluid particle density and taking $\mathbf{v}_s$ purely in the x direction, one may write for small v_s:

$$F(v_s)\approx F_0+\tfrac{1}{2}L_xL_y\rho_s m v_s^2, \tag{9}$$

from which immediately follow the expressions for the superfluid momentum density:

$$m\rho_s v_s=\frac{1}{L_xL_y}\frac{\partial F(v_s)}{\partial v_s}, \tag{10}$$

and the superfluid particle density

$$\rho_s=\frac{1}{L_xL_y}\frac{1}{m}\frac{\partial^2F(v_s)}{\partial v_s^2}. \tag{11}$$

It is clear from Eq. (6) that the lowest velocity must correspond to $n=1$ and consequently, for v_s to be small enough to justify Eq. (9), the system must be large. Equation (11) is often expressed in words by saying that the superfluid density is the curvature of the free energy as a function of the superfluid velocity. That this is not quite true is clear from Eq. (6) and Fig. 1 which together emphasize that ρ_s is the curvature of the parabola passing through the first few local minima of the free energy as a function of v_s. However, for brevity, we shall refer to this as the curvature of the free energy.

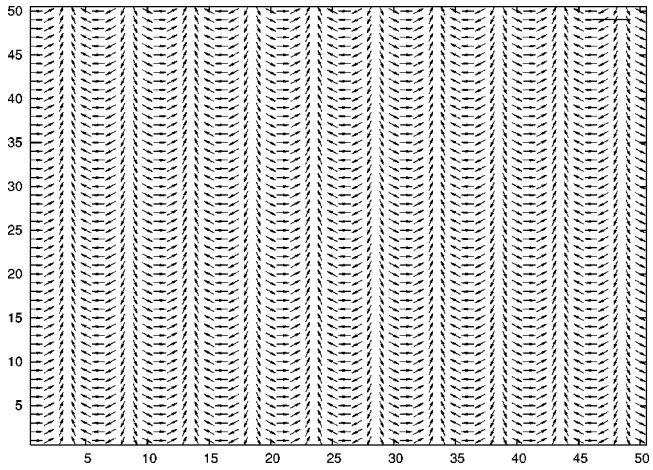

FIG. 2. Configuration with $v_s=n\kappa_0$, $n=5$ on a 50×50 lattice. This configuration satisfies the velocity quantization condition and locally minimizes the free energy for $n=5$ at $T=0$. The direction of the arrows gives the value of θ_i.

Recalling that $F=-\ln Z/\beta$, it is easy to apply Eqs. (10) and (11) to the *XY* model and obtain

$$\frac{\partial F}{\partial v_s}=\left\langle\sum_{\langle i,j\rangle:x}\sin(\theta_i-\theta_j)\right\rangle, \tag{12}$$

$$\frac{\partial^2F}{\partial v_s^2}=\beta\left\{\left\langle\sum_{\langle i,j\rangle:x}\sin(\theta_i-\theta_j)\right\rangle^2-\left\langle\left(\sum_{\langle i,j\rangle:x}\sin(\theta_i-\theta_j)\right)^2\right\rangle\right\}+\left\langle\sum_{\langle i,j\rangle:x}\cos(\theta_i-\theta_j)\right\rangle, \tag{13}$$

where the notation $\langle i,j\rangle:x$ means the sum is performed over nearest neighbors only in the x direction (since we took v_s to be in that direction). Equation (12) allows the determination of ρ_s in a *nonequilibrium flow situation*, while Eq. (13) gives ρ_s also at equilibrium where $v_s=0$. Note, from Eqs. (10) and (12), that the superfluid velocity v_s is proportional to $\Sigma_{\langle i,j\rangle:x}\sin(\theta_i-\theta_j)$. For low velocities we have $v_s\propto\Sigma_{\langle i,j\rangle:x}(\theta_i-\theta_j)$ which satisfies the velocity quantization condition, Eq. (6), and is illustrated in Fig. 2 for $n=5$.

III. NONEQUILIBRIUM SIMULATIONS

A. Metastability and superfluid density

In this section we study some of the nonequilibrium properties of the two-dimensional *XY* model. In particular, we are interested in the transitions among the local minima of Fig. 1, in other words the onset of dissipation in the superflow and its relation to the critical velocity and thermodynamic stability of the superfluid. The transitions between the local minima are driven by thermal fluctuations as the system attempts to minimize its free energy. Different simulation al-

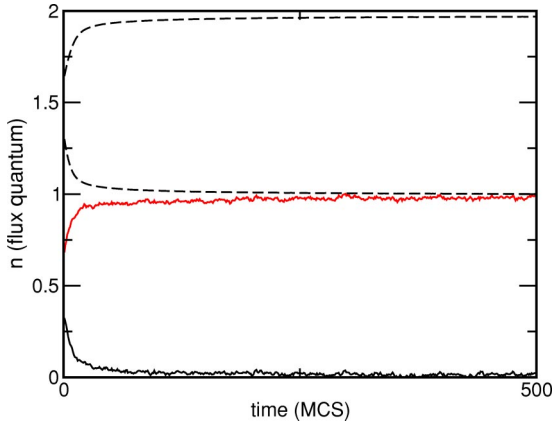

FIG. 3. The flux quantum, n as a function of time in Monte Carlo Sweeps (MCS) for 100×100 system at $T=0.25<T_{\mathrm{KT}}$. We see that n flows to the nearest integer value clearly exhibiting the Meissner effect and velocity quantization.

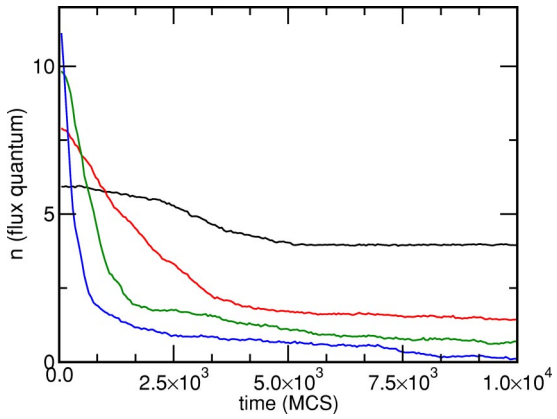

FIG. 4. The flux quantum n vs MCS for 100×100 system at $T=0.5$. It is clear that the final value of n depends on the initial value: It is not necessary for the system always to tunnel to the $n=0$ state, nor does it have to tunnel from n to $n-1$. The initial values for the flux are $n=6$, 8, 10, and 12.

gorithms will lead to different lifetimes of the metastable states. However, the scaling of these lifetimes with the geometry of the system and the velocity of the superfluid will be the same. We chose to use the single spin flip local Metropolis algorithm. We shall see below that agreement with experiments is very good.

Nonequilibrium simulations are performed by placing the system in initial configurations corresponding to flow at a chosen initial superfluid velocity. Equation (5) shows that the superfluid flows if there is a phase gradient, while Eq. (6) places a condition on the allowed values of v_s. Figure 2 shows an initial configuration corresponding to a flowing superfluid with flux $n\kappa_0=5\kappa_0$. It is also clear that this configuration corresponds to irrotational flow.

We first show that superfluid flow in the two dimensional XY model is (meta)stable by demonstrating the existence of the Meissner effect and velocity quantization. As discussed in Sec. I, if the initial n is less the $1/2$, a "stable" superfluid will satisfy velocity quantization by coming to rest thus exhibiting the Meissner effect. On the other hand, if $n>1/2$, the system will evolve to the nearest integer value of n changing its velocity in the process. Figure 3 shows simulation results for four initial values of the flux quantum, $n=0.4$, 0.6, 1.4, and 1.6 for a 100×100 system at $T=0.25<T_{\mathrm{KT}}$. The behavior of single configurations is shown for $n=0.4$ and 0.6 while for $n=1.4$ and $n=1.6$ we show averages over 1000 configurations (the dashed lines). The figure shows clearly that the Meissner effect and velocity quantization are both present in the two dimensional XY model below T_{KT}. This means that the free energy does indeed have the form depicted in Fig. 1 otherwise there would be no reason for the flux quantum to get stuck at integer values as shown in Fig. 3.

That integer flux configurations are metastable, rather than stable, is shown in Fig. 4 where transitions are seen. It is also clear from this figure that transitions do not always change the flux by the same amount. The change in the flux, and consequently dissipation and the final metastable or stable configuration, depend on the starting value: The larger the initial flux, the larger the change and, consequently, the smaller the value of the final flux. The reason for this will be discussed below where we will study these transitions in more detail. Such transitions between local minima, also referred to as phase slips, have been observed experimentally.[16]

We now compare the superfluid density using equilibrium and nonequilibrium measurements. The equilibrium measurements were done, as usual, by using Eq. (13) and random initial configurations with $n=0$. The nonequilibrium measurements were performed by putting the system in an $n=1$ initial configuration and using Eqs. (10) and (12) to measure the superfluid density. For $T<0.7$ the $n=1$ metastable state is so long lived that even after ten million sweeps the transition does not occur (for 128×128 system). For such long lived states the measurements are simply performed as if the system is in an equilibrium configuration. However, as T_{KT} is approached, the lifetime of the metastable state becomes very short and more care must be taken. In this temperature range we measure the superfluid density as follows. The system is put in the $n=1$ initial configuration and its evolution is followed until it makes the transition to the $n=0$ configuration, performing measurements every few sweeps. This is done many times for the same temperature (40–300 times); of course the transition time can be very different from one simulation to another at the same T (this will be discussed below). The superfluid momentum density,[26] $\rho_s v_s$, from all the runs for the same temperature is then histogrammed to decide if it is even meaningful to calculate an average of this quantity. The results for two temperatures are shown in Fig. 5. The relative heights of the peaks are not important since the height of the peak at $\rho_s v_s=0$ depends on how long the simulation is allowed to run after the transition has taken place. What is important is the height of the peak at nonzero momentum compared to its width and also compared to the height of the histogram in the transition region between the two peaks. It is clear that for the upper panel of Fig. 5, it is meaningless to calculate the superfluid momentum in the metastable state, while for the lower panel this quantity is well defined.

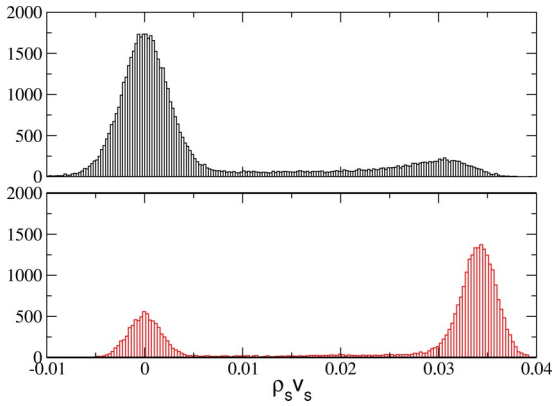

FIG. 5. Histogram of the superfluid momentum for a system of size 128×128. Upper panel: $T=0.9$ and 45 simulations. Lower panel: $T=0.825$ and 30 simulations.

With the help of such analysis we calculate ρ_s in the nonequilibrium situation and compare with the equilibrium values in Fig. 6. The agreement is excellent which demonstrates numerically the correctness of this approach. For $T>0.875$, we can no longer extract ρ_s this way: the initial superfluid velocity, $v_s=2\pi/L_x$ (in units of $\hbar/m$ and for $L_x=128$) is greater than the critical velocity at these temperatures and the superfluid kinetic energy is quickly dissipated. In order to get closer to T_{KT}, the initial v_s must be smaller which is impossible for this system size since already $n=1$. To achieve lower v_s, a larger system would be needed; this is another demonstration of the important interplay between system size and v_s.

Note, that the excellent agreement between the equilibrium and nonequilibrium measurements of ρ_s (which we have also verified with simulations at higher velocities) does not support Eq. (11) of Ref. 23 which claims a strong dependence of ρ_s on v_s.

An interesting aspect of the nonequilibrium measurements of ρ_s is the possibility of getting direct evidence for the universal jump condition:[25]

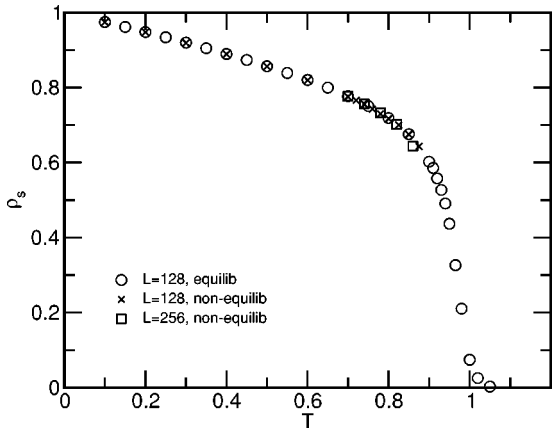

FIG. 6. The superfluid density, ρ_s (in units of $m/\hbar^2$), from equilibrium and nonequilibrium measurements vs T. The error bars are smaller than the symbols.

$$\rho_s(T_{\mathrm{KT}})=\frac{2}{\pi}T_{\mathrm{KT}}. \tag{14}$$

In Ref. 27 a method based on higher order derivatives of the free energy was presented as a way for direct detection of this jump. In the present method, it is clear that when the system is close enough to T_{KT} the superfluid momentum will simply vanish discontinuously. Already for $L=128$, this happens for T just above 0.875 (the last nonequilibrium point shown in Fig. 6), whereas $T_{\mathrm{KT}}\approx0.9$.

B. Vortices and dissipation

We now turn to the dissipation mechanism, i.e., the excitations which take the system from one local minimum to another. Onsager[14] and Feynman[17] argued that the creation of large vortices in the flowing superfluid was responsible for these dissipative transitions. Although the general features of this idea are widely accepted, disagreement remains on the details. Here we shall study and confirm numerically that, in the two-dimensional XY model, transitions between the metastable persistent flow states proceeds via the formation of large vortex–antivortex pairs oriented orthogonally to the direction of flow. We will describe how it happens and study its dependence on the width of the system and the flux velocity.

Our numerical simulations demonstrate that, for $T<T_{\mathrm{KT}}$, thermal fluctuations take place in such a way that the large scale band structures, Fig. 2, are maintained due to the spin stiffness. As individual spins undergo thermal fluctuations, the bands of approximately parallel spins fluctuate as large scale elastic objects maintaining their large scale form and spanning the system (in the y direction by choice). Deformations of these elastic objects cost energy proportional to the curvature of the deformation and to the spin stiffness, i.e., ρ_s. Eventually, two bands whose spins differ by 2π are deformed enough to touch. When this happens, the 2π difference between these bands loses its meaning where they touch, but away from the contact region the difference still exists. This topological ambiguity is in fact the vortex–antivortex excitation which can trigger the transition. This situation is shown in Fig. 7 which is a snapshot of the system depicted in Fig. 2 at $T=1/3$ after 1100 Monte Carlo sweeps. The square in Fig. 7 shows where two bands of spin differing by 2π have touched. A vortex is visible just below the square and an antivortex just above it; also visible is a flux line going down from the vortex and connecting it to the antivortex (we have periodic boundary conditions). In two dimensions, for $T<T_{\mathrm{KT}}$, the energy of such excitations is of the order of $\ln r$, where $r\approx L_y$ is the separation of the vortex–antivortex pair.

When such contact is made, it may be very difficult to break and dissipation of a flux quantum can then proceed by zipping together the two bands into a single one thus eliminating a quantum of flux. The reason for this is that for $T<T_{\mathrm{KT}}$ the vortices are confined. It is favorable for a vortex to find an antivortex and annihilate. In the situation of Fig. 7, the logarithmic confining potential will pull them together with the vortex moving down and the antivortex moving up

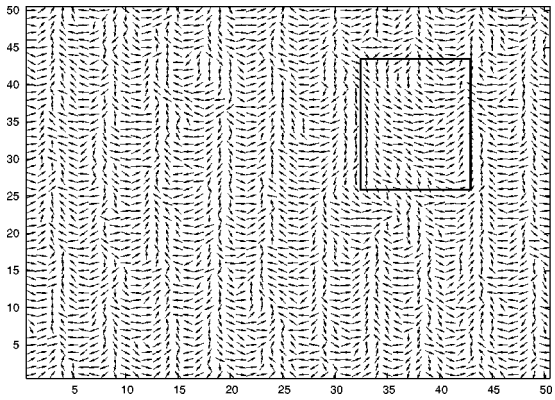

FIG. 7. The configuration in Fig. 2 after 1100 MCS at $T=1/3$. The square shows the region where two bands of spins differing by 2π have merged. A vortex (antivortex) can be seen below (above) the square.

to meet and annihilate zipping the the two bands in their wake. In the case of nonperiodic boundary conditions in the y direction, the vortex and antivortex will each be attracted to its image thus moving outward and crashing against the wall. The outcome, in both cases, is that the two bands are zipped together and a quantum of flux disappears, i.e., dissipates.

Note that this mechanism, while involving vortices, is not quite the same as that discussed in Ref. 22. In Ref. 22, the vortex is assumed to nucleate at a singular point where the wave function vanishes, $|\psi| \rightarrow 0$, which implies a vanishing density at that point. In the mechanism discussed here, only the phase, modeled by the angles θ, fluctuates: The transitions here are caused by phase, not density, fluctuations.

The role of the velocity is now straightforward to describe qualitatively. The higher the velocity, the more closely packed the bands become and thus the higher the likelihood that more than one contact region be established. Consequently, several vortex–antivortex pairs may be created with the result that the transition can dissipate more than one flux quantum. This explains what is observed in Fig. 4 where it is seen that more flux quanta are dissipated if the initial velocity is higher. If the velocity is very high, so many vortices are created that the transition is essentially immediate.

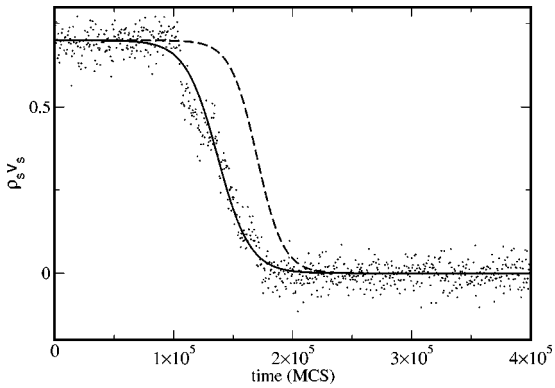

FIG. 8. The superfluid momentum vs time in Monte Carlo steps for a 128×128 system at $T=0.83$. The line is a fit of the form $\rho_s v_s = a\{1-\tanh[b(t-\tau_{\rm esc})]\}$. The dashed line is a fit to the transition of another configuration which is not shown for clarity.

It is interesting to note that whereas the superflow is in general irrotational, this is no longer the case while the system is undergoing a transition. This is clearly seen in Fig. 7 where one observes sheer in the flow: The $\hat{x}$ flow velocity in the zones where the two bands have not yet touched is larger than that where contact has been established thus producing sheer at the interface.

Before discussing the scaling of the lifetime of the metastable states, we first show that the escape time from a local minimum is well defined and may be measured accurately. Figure 8 shows a typical evolution of the superfluid momentum as a function of time in Monte Carlo steps (MCS). The solid line is a fit of the form $\rho_s v_s = a\{1-\tanh[b(t-\tau_{\rm esc})]\}$ which allows us to measure the lifetime, $\tau_{\rm esc}$, of the initial metastable state. The dashed line is a fit of the same form to the evolution of another configuration which we do not show. We shall return to this figure in the next subsection.

As mentioned in Sec. I, the critical velocity of superfluid helium passing through orifices *decreases* as the opening size is *increased*. Here we show that similar behavior is exhibited by the two dimensional *XY* model. In Fig. 9 we show as a function of the width of the system, L_y, the average time (in MCS) to make a transition from the n to the $n-1$ state for $T=0.25$ and 0.5. We see that, for $L_y \geqslant 32$, τ decreases as a power law as the system gets wider. This decrease in τ with increasing L_y may be understood qualitatively with the help of the mechanism shown in Fig. 7. Increasing L_y makes it easier, at constant spin stiffness, to bend the spin bands by the needed amount to make them touch since the *curvature* is smaller the larger the L_y. However, a straightforward application of thermal activation arguments fails to give the observed behavior. The energy of a vortex–antivortex pair in a the superfluid flow field is given by[23]

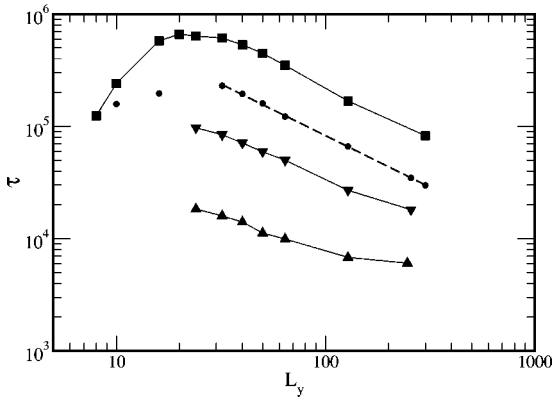

FIG. 9. The average lifetime τ (MCS) vs L_y for $8 \leqslant L_y \leqslant 300$ and $L_x=128$. The transitions are from $n=7$ to $n=6$ (up triangles), $n=6$ to $n=5$ (down triangles), $n=5$ to $n=4$ (squares). For these cases $T=0.5$. Circles: transition from $n=12$ to $n=11$ at $T=0.25$. The averages are calculated over between 50 and 10^3 realizations. The dashed line is a fit giving $\tau = 5.7\times10^6/L_y^{0.9}$, the solid lines are to guide the eye.

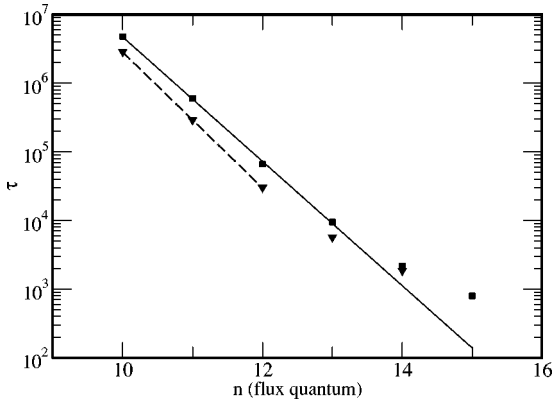

FIG. 10. The average lifetime of metastable states vs the flux quantum, n, for 128×128 (squares) and 128×130 (triangles) systems at $T=0.25$. The solid line is $\tau=5.4\times10^{15}\exp(-2n)$, the dashed line is $\tau=1.9\times10^{16}\exp(-2.276n)$.

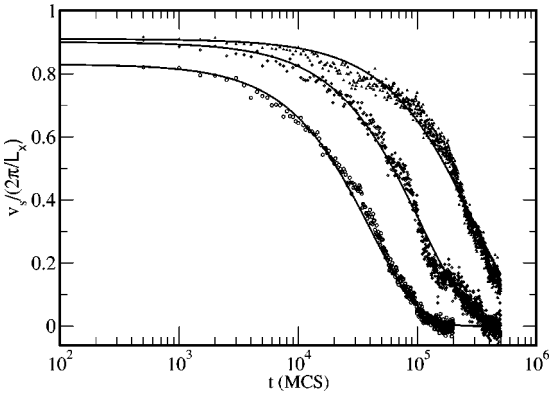

FIG. 11. Superfluid velocity vs time averaged over several realizations for a 128×128 system. Lowest curve: $T=0.92$, 100 realizations, middle curve: $T=0.875$, 30 realizations and upper curve: $T=0.85$, 30 realizations.

$$E = 2\pi\rho_s \ln L_y - (2\pi)^2\rho_s n\frac{L_y}{L_x}, \tag{15}$$

where the distance between the vortex and antivortex is taken to be L_y as is seen in Fig. 7 and the superfluid velocity is $2n\pi/L_x$. This gives a transition rate[13]

$$r = \nu_0 L_y e^{-\beta E}, \tag{16}$$

where ν_0 is the attempt rate. The average lifetime is then

$$\tau \sim L_y^{2\pi\rho_s\beta-1} e^{-\beta\rho_s n(2\pi)^2 L_y/L_x}. \tag{17}$$

This result which predicts an exponential decay of τ with L_y does not agree with the observed numerical results.[28] For very narrow systems, $L_y=8$, 10, and 16 in Fig. 9, it is seen that τ does not decrease with increasing L_y. This is because the system is becoming one dimensional in which case the spins are not stiff and therefore $\tau\to0$.

Figure 10 shows the dependence of τ on $v_s=2\pi n\kappa_0$. The metastable states (i.e., persistent superflow) are shorter lived for larger velocities, v_s, which is in agreement with experiments. The exponential decay with increasing velocity appears in Eq. (17) but with an exponent which is too large. For the larger values of n, the decay is no longer exponential because local minima become too shallow and also because the simultaneous dissipation of flux quanta becomes more important.

C. Comparison with experiments

Decay of persistent currents has been studied both in bulk and films. The results of Refs. 29–31 were found to be consistent with time dependence of the superfluid velocity in the form

$$v_s = A - B\ln t, \tag{18}$$

where A and B are empirical constants. In other words, the observed dissipation was very slow. However, Ref. 13 observed both slow and fast dissipation, the former well described by Eq. (18) while the latter much better described by

$$v_s = \frac{A_1}{(1+B_1 t)^r}, \tag{19}$$

where A_1, B_1, and r are empirical constants. Equation (18) fails to describe the fast decays.

In this section we shall compare the dissipation in the XY model with these experimental results. Figure 8 shows, for one configuration, the superfluid momentum as a function of time clearly displaying the dissipation of kinetic energy. The behavior in this figure follows neither Eq. (18) nor (19) and does not resemble Figs. 6 or 7 of Ref. 13 (see Figs. 13 and 14 in this paper). However, Fig. 8 shows the behavior of only one configuration dissipating exactly one flux quantum whereas in the experiments one presumably observes an average of such processes. In other words, the experimental situation represents many different regions of quantized flux making transitions at different times. What is observed then is the average dissipation as a function of time. To test this idea, we performed simulations of the type shown in Fig. 8 but averaging over many configurations. Three such averages are shown by the points in Fig. 11. This figure strongly resembles Fig. 6 of Ref. 13 and the data are reasonably well described by Eq. (19) (not shown in the figure, the curves shown will be discussed below). We therefore see that, at least for fast dissipation, the XY model is in very good qualitative agreement with experiments adding support to the phase zipping dissipation mechanism discussed above. Slow dissipation is harder to study numerically because for long escape time it takes many more realizations to get good statistics. However, the simulations we performed for this case are also consistent with the experiments.

To model the numerically observed time dependence of v_s displayed in Fig. 11, one must examine the distribution of escape times, $\tau_{\rm esc}$, at a given T and v_s. One such distribution is shown in Fig. 12. The solid curve is a fit of the form

$$P(\tau_{\rm esc}) = A\tau_{\rm esc}^{\alpha} e^{-\gamma\tau_{\rm esc}}, \tag{20}$$

where A, α, and γ are fitting parameters. For the case of Fig. 12, $\alpha=3.7$ and $\gamma=3.1\times10^{-4}$. The average superfluid velocity, $\overline{v_s}$, is then given by

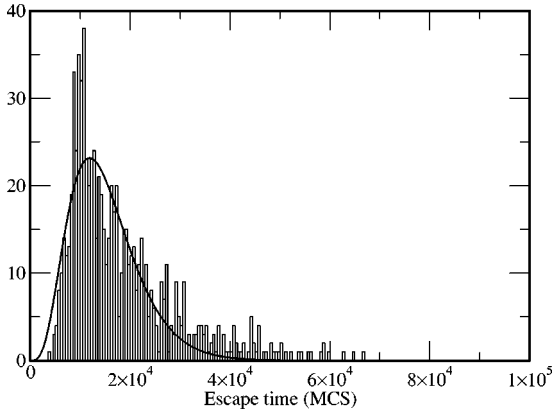

FIG. 12. The distribution of escape times from $n=6$ to $n=5$ for a 128×128 system at $T=0.5$. The solid curve is a fit of the form Eq. (20).

$$\overline{v_s}(t) = \int_0^\infty d\tau_{\rm esc} v_s(t) P(\tau_{\rm esc}) \tag{21}$$

where $P(\tau_{\rm esc})$ is normalized and where $v_s(t)$ may be taken of the form discussed in Fig. 8. However, to simplify the discussion and allow exact integration of Eq. (21), we may take $v_s(t)=v_s(0)\Theta(\tau_{\rm esc}-t)$ where Θ is the Heaviside function. Equation (21) then reduces to

$$\overline{v_s}(t) = A\int_t^\infty d\tau_{\rm esc}\tau_{\rm esc}^\alpha e^{-\gamma\tau_{\rm esc}} = A'\Gamma(1+\alpha,\gamma t), \tag{22}$$

where $\Gamma(1+\alpha,\gamma t)$ is the incomplete gamma function, A', α, and γ are fitting parameters. The solid curves in Fig. 11 are fits to the numerical data using Eq. (22) with $(\alpha=0.08,\gamma=2.77\times10^{-5})$ for the lowest curve $(\alpha=0.04,\gamma=10^{-5})$ for the middle curve and $(\alpha=0.02,\gamma=3.5\times10^{-6})$ for the top curve. We see that agreement with the numerical results is excellent. As a further test of these ideas, in Fig. 13 we show a fit to the experimental data in Fig. 6 of Ref. 13 using Eq. (22). The curve agrees remarkably well with the experimental data, in fact much better than Eq. (19), see Fig. 6 in Ref. 13.

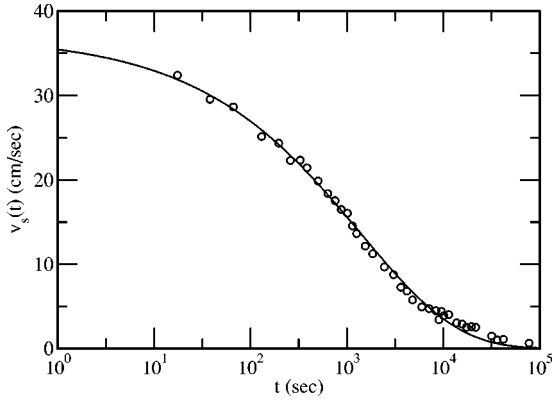

FIG. 13. Superfluid velocity vs time. The circles are the experimental data for superfluid films in Fig. 6 of Ref. 13. The solid curve is a fit using Eq. (22). The fitting parameters are $(\alpha=0,\gamma=0.043)$.

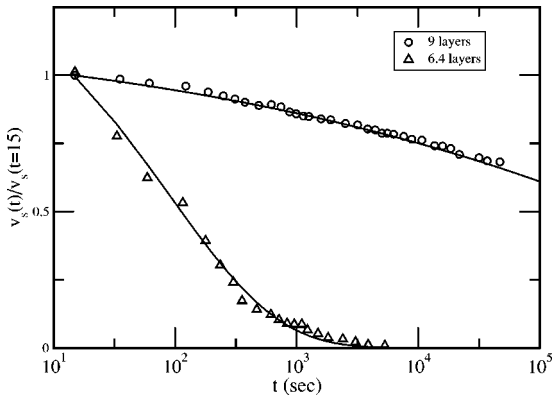

FIG. 14. Superfluid velocity vs time for films with different thickness at $T=1.45$ K. The symbols are experimental data from Fig. 7 of Ref. 13. The solid curves are fits using Eq. (22). For 6.4 layers $(\alpha=0.3,\gamma=0.5)$ and for nine layers $(\alpha=-0.73,\gamma=0.001)$

The escape time distribution, Eq. (20), used in this analysis is reasonable for fast to medium dissipation as can be seen in Fig. 12. However, it is not clear that the same distribution gives a reasonable description for extremely long lived persistent flows of the type well modeled by Eq. (18). In other words, the question is whether for very slow decays Eq. (22) behaves like the experimental results, i.e., roughly linearly in $\ln t$. To verify this, we show in Fig. 14 fits of Eq. (22) to two data sets from Fig. 7 of Ref. 13. We see that even for the slowest dissipation reported, Eq. (22) gives very good agreement with experiments. For the slow decay, though, it was necessary to take $\alpha<0$ to get a good fit. This might cause concern in view of Eq. (20) which would then diverge for $\tau_{\rm esc}=0$. However, negative α is needed only for the very slow decays where $\tau_{\rm esc}$ is never zero. In fact the distribution of escape times for slow dissipation will most likely have a lower cutoff below which no dissipation is observed. Note from Eq. (20) that γ^{-1} is a measure of the lifetime of the metastable states. The values obtained from the fits in Fig. 14 are $\gamma^{-1}\approx2$ s for the fast decay and $\gamma^{-1}\approx10^3$ s for the slow one.

This discussion supports the view that the experimentally observed dissipation curves are averages over many events like the one shown in Fig. 8 with an escape time distribution similar to Fig. 12.

IV. CONCLUSIONS

We have presented a first study of the two-dimensional planar *XY* model in topologically nontrivial metastable states. These *twisted* states represent a two-dimensional superfluid under nonequilibrium *persistent flow* conditions which satisfy the superfluid velocity quantization condition, Eq. (6). Transitions among these states change the topological quantum number, the quantized flux, and represent the dissipation of flux quanta in a flowing superfluid which is related to its critical velocity. The properties of these transitions were studied in particular their dependence on the geometry of the system and the superfluid velocity. We showed that, in agreement with experimental results, the metastable

states have shorter lifetimes and, therefore, lower critical velocities when the width of the system increases. Also in agreement with experiments, we showed that dissipation is more rapid the higher the initial superfluid velocity. The dissipation mechanism was identified and studied: When two bands of spin differing by 2π deform and touch due to thermal fluctuations, a bound vortex–antivortex pair of length L_y is created. The confining force pulls the vortex and antivortex towards each other thus zipping together the two touching bands of spin into a single band.

Using this mechanism and a functional form for the escape time distribution motivated by the numerical results, we calculated the average superfluid velocity, $\overline{v_s}(t)$, and showed it to be in excellent agreement both with our numerical simulations (Fig. 11), and with the experimental results of Ref. 13 (Figs. 13 and 14). This provides support for the view that the dissipation observed experimentally is an average over several regions with, possibly, different velocities where dissipation of flux quanta takes place independently and at different times.

It is interesting that the two dimensional planar *XY* model, with no condensate and no linear dispersion for the low-lying excitations still exhibits (meta)stable superfluid flow and agrees well with experimental results.

Finally we mention that the free energy landscape may be studied directly using, for example, the Wang-Landau[32] algorithm. Integer windings in the two dimensional *XY* model were addressed in Ref. 33. Very recently,[34] different topological sectors and the helicity modulus were studied for the four dimensional compact $U(1)$ lattice gauge theory.

ACKNOWLEDGMENTS

The author acknowledges very helpful discussions with E. L. Pollock, B. Militzer, R. T. Scalettar, M. Troyer, Ph. de Forcrand, and T. Ramstad. He also thanks the Norwegian University of Science and Technology, the Complex Group and Norsk Hydro for their hospitality and generosity during a sabbatical stay. This work was supported by the NSF-CNRS Cooperative Grant No. 12929.

*Permanent address.
[1] M.-O. Mewes *et al.*, Phys. Rev. Lett. **77**, 416 (1996).
[2] M. H. Anderson *et al.*, Science **269**, 198 (1995).
[3] E. Kim and M. H. W. Chan, Nature (London) **427**, 225 (2004).
[4] L. Landau, J. Phys. (USSR) **5**, 71 (1941); **11**, 91 (1947).
[5] L. D. Landau and E. M. Lifshitz, *Statistical Physics* (Pergamon, New York, 1969), Sec 67.
[6] L. Bruschi, P. Mazzoldi, and D. Santini, Phys. Rev. Lett. **21**, 1738 (1968).
[7] W. J. Trela and W. M. Fairbank, Phys. Rev. Lett. **19**, 822 (1967).
[8] A. J. Leggett, Rev. Mod. Phys. **71**, S318 (1999).
[9] A. J. Leggett, in *Topics in Superfluidity and Superconductivity, in Low Temperature Physics*, Proceedings of Blydepoort South Africa, 1991, edited by M. J. R. Hoch and R. H. Lemmer (Springer–Verlag, 1991).
[10] What this means will become clear shortly.
[11] G. B. Hess and W. M. Fairbank, Phys. Rev. Lett. **19**, 216 (1967).
[12] S. C. Whitmore and W. Zimmermann, Jr., Phys. Rev. Lett. **15**, 389 (1965).
[13] D. T. Ekholm and R. B. Hallock, Phys. Rev. B **21**, 3902 (1980).
[14] L. Onsager, Nuovo Cimento, Suppl. **6**, 249 (1949).
[15] P. C. Hohenberg and P. C. Martin, Ann. Phys. (N.Y.) **281**, 637 (2000).
[16] A. Amar, Y. Sasaki, R. L. Lozes, J. C. Davis, and R. E. Packard, Phys. Rev. Lett. **68**, 2624 (1992).
[17] R. P. Feynman, *Progress in Low Temperature Physics* (North-Holland, Amsterdam, 1955), Vol. I, Chap. II.
[18] H. G. Evertz and D. P. Landau, Phys. Rev. B **54**,12302 (1996).
[19] D. J. Bishop and J. D. Reppy, Phys. Rev. Lett. **40**, 1727 (1978).
[20] M. H. W. Chan, A. W. Yanof, and J. D. Reppy, Phys. Rev. Lett. **32**, 1347 (1974).
[21] S. V. Iordanskii, JETP Lett. **21**, 467 (1965).
[22] J. S. Langer and M. E. Fisher, Phys. Rev. Lett. **19**, 560 (1967).
[23] B. A. Huberman, R. J. Myerson, and S. Doniach, Phys. Rev. Lett. **40**, 780 (1978).
[24] V. Ambegaokar, B. I. Halperin, D. R. Nelson, and E. D. Siggia, Phys. Rev. B **21**, 1806 (1980).
[25] D. R. Nelson and J. M. Kosterlitz, Phys. Rev. Lett. **39**, 1201 (1977).
[26] We use v_s in units of $\hbar/m$, see Eq. (5).
[27] P. Minnhagen and B. J. Kim, Phys. Rev. B **67**, 172509 (2003).
[28] Note that the exponent of the prefactor L_y is always positive for $T<T_{KT}$ where superfluidity exists.
[29] J. S. Langer and J. D. Reppy, *Progress in Low Temperature Physics*, edited by C. J. Gorter (Noth-Holland, Amsterdam, 1970), Vol. 6, p. 1.
[30] H. Kojima, W. Veith, E. Guyon, and I. Rudnick, *Low Temperature Physics*, edited by K. D. Timmerhaus, W. J. O'Sullivan, and E. F. Hammel (Plenum, New York, 1974), Vol. 1, p. 239.
[31] K. L. Telschowand, R. B. Hallock, Phys. Rev. Lett. **37**, 1484 (1976).
[32] F. Wang and D. P. Landau, Phys. Rev. E **64**, 056101 (2001).
[33] G. G. Batrouni, T. Ramstad, and A. Hansen, Philos. Trans. R. Soc. Ser. A (to be published).
[34] M. Vettorazzo and Ph. de Forcrand, Nucl. Phys. B **686**, 85 (2004).